

Modern Physics Letters A
 © World Scientific Publishing Company

Estimate of the magnetic field strength in heavy-ion collisions

V. V. SKOKOV

*Gesellschaft für Schwerionenforschung mbH, Planckstr. 1, D-64291 Darmstadt, Germany
 Frankfurt Institute for Advanced Studies, Universität Frankfurt, D-60438 Frankfurt am Main,
 Germany*

Joint Institute for Nuclear Research, RU-141980 Dubna, Moscow Region, Russia

A. Yu. ILLARIONOV

Dipartimento di Fisica dell'Università di Trento, via Sommarive 14, I-38050 Povo, Trento, Italy

V. D. TONEEV

*Gesellschaft für Schwerionenforschung mbH, Planckstr. 1, D-64291 Darmstadt, Germany
 Joint Institute for Nuclear Research, RU-141980 Dubna, Moscow Region, Russia*

Received (Day Month Year)

Revised (Day Month Year)

Magnetic fields created in the noncentral heavy-ion collision are studied within a microscopic transport model, namely the Ultrarelativistic Quantum Molecular Dynamics model (UrQMD). Simulations were carried out for different impact parameters within the SPS energy range ($E_{lab} = 10 - 158A$ GeV) and for highest energies accessible for RHIC. We show that the magnetic field emerging in heavy-ion collisions has the magnitude of the order of $eB_y \sim 10^{-1} \cdot m_\pi^2$ for the SPS energy range and $eB_y \sim m_\pi^2$ for the RHIC energies. The estimated value of the magnetic field strength for the LHC energy amounts to $eB_y \sim 15 \cdot m_\pi^2$.

Keywords: heavy-ion collisions, quark-gluon plasma

PACS Nos.: 25.75.-q, 25.75.Ag

1. Introduction

Heavy-ion collisions are intensively investigated both experimentally and theoretically to reveal information about properties of the nuclear matter under extreme conditions. Heavy-ion collision experiments at AGS (BNL), SPS (CERN) and RHIC (BNL) as well as future ones planned at FAIR (GSI), NICA (JINR), LHC (CERN) make it possible to explore the phase diagram of the nuclear matter in a broad parameter range of temperature and baryon density. One of the most important issue addressed in nucleus-nucleus collisions is the possibility for nuclear matter to undergo phase transitions into a new state of matter. At least two of these transitions, chiral and deconfinement, are commonly expected. Though at zero baryon chemical potential both transitions seem to have the same critical temperature, it is not clear

at the moment whether this situation will remain at the large chemical potential or the the chiral phase transition anticipates the deconfinement one, allowing for the “quarkyonic” states ^{1,2} with the massless confined quarks. Despite the recent progress ^{3,4}, the lattice QCD calculations at finite baryon chemical potential do not provide fully reliable information on the subject.

One of the most exciting signals of the deconfinement and the chiral phase transitions in heavy-ion collisions, the chiral magnetic effect, suggested in ⁵, predicts the preferential emission of charged particles along the direction of angular momentum in the case of the noncentral heavy-ion collisions due to the presence of nonzero chirality. As it was stressed in ^{5,6}, both the deconfinement and chiral phase transitions are the essential requirements for the chiral magnetic effect to take place. The first one is needed, since only in this case the soft quarks can be separated by a distance larger than the radius of a nucleon. The second one is also required ^{5,6}, since nonzero values of the chiral condensate drive asymmetry between the number of right- and left-handed quarks to zero.

The effects caused by a strong magnetic field are not limited by the chiral magnetic effect ⁶. They include also the induced chiral symmetry breaking ⁷, modification of the nature of the chiral phase transition (e.g. turning the crossover phase transition to the first-order one through influence on the chiral condensate ^{8,9,10,11,12,13}), influence on the possible color-conducting phases ^{14,15,16} and the pion condensate ¹⁷, spontaneous creation of the axial currents ^{18,19}, and formation of the π_0 -domain walls ²⁰. Recently, the effect of a large magnetic field on the sound velocity of a propagating plane wave was studied in Ref. ²¹.

The key quantity of these effects is a magnitude of the background magnetic field strength created in heavy-ion collisions. The early estimate of the magnetic field for the RHIC energy was made in Ref. ⁵. It was shown that the field may reach very high values $eB \sim 3 \cdot m_\pi^2 \sim 3 \times 10^{18}$ Gauss^a. The aim of this article is to improve a qualitative estimate, make the quantitative calculation of the magnetic field for heavy-ion collisions at different impact parameters and different energies, study its characteristics. The calculations will be carried out within the microscopic transport model, namely the Ultrarelativistic Quantum Molecular Dynamics model (UrQMD), and will be complemented by analytical considerations.

2. Magnetic field in heavy-ion collisions

The Ultrarelativistic Quantum Molecular Dynamics model is a microscopic model used to simulate (ultra)relativistic heavy-ion collisions in the energy range from Bevalac and SIS up to AGS, SPS and RHIC. The detailed description of the model can be found in Refs. ^{22,23}.

In this paper we focus our investigation on the magnetic field evaluated in the center of the created fireball and on the energy density of nuclear matter in the

^aProbably the first rough estimate of the magnetic field in heavy-ion collision was made in Ref. ¹⁷

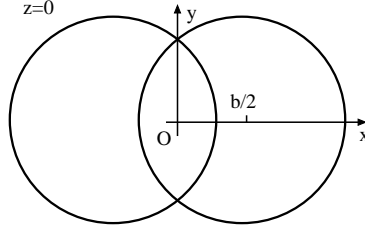


Fig. 1. The transverse plane of a noncentral heavy-ion collision. The impact parameter of the collision is b . The magnetic field is to be calculated at the origin O and along the y -axis.

region surrounding this point.

The magnetic field strength at a position \vec{x} and time t is defined by the Lienard-Wiechert potentials

$$e\vec{B}(t, \vec{x}) = \alpha_{\text{EM}} \sum_n Z_n \frac{1 - v_n^2}{(R_n - \vec{R}_n \vec{v}_n)^3} [\vec{v}_n \times \vec{R}_n], \quad (1)$$

where the fine-structure constant $\alpha_{\text{EM}} \approx 1/137$, Z_n is an electric charge of the n th particle (in units of the electron charge) and $\vec{R}_n = \vec{x} - \vec{x}_n$ is a radius vector of particle, \vec{v}_n is a particle velocity. The quantities \vec{v}_n and \vec{x}_n are taken at the time moment t' retarded with respect to the observation time t to be defined implicitly by the following equation

$$|\vec{x} - \vec{x}_n(t')| + t' = t, \quad (2)$$

where we use the natural units and set $c = 1$. Summation is to be carried out over all charged particles. However, to avoid uncertainties coming from participant contribution, the summation was performed only over the spectators in our calculations.

In principle, the magnetic field can be calculated for any space points. We limit ourselves only to evaluation of the field at the central point of the reaction volume O (see Fig. 1) and the dependence on y -coordinate at $z = x = 0$.

On the basis of the expression (1) let us draw several conclusions for the main properties of the magnetic field at the origin O . First of all, it is evident from symmetry reasons that the magnetic field will be negligible for a collision with a small impact parameter. From the same symmetry considerations one obtains that the field will have only nonzero B_y -component. Second, the field will be negligible for low bombarding energies because the field strength is proportional to the particle velocity. On the other hand, for very high ultrarelativistic energies of a collision the contribution to the magnetic field is feasible only for particles close to the transverse plane $(R_n - \vec{R}_n \vec{v}_n) \sim 0$. The contribution from particles away from the transverse plane is suppressed by the factor $(1 - v^2)$. From the expression (1) it also follows that the characteristic magnetic field dependence on nuclei charge is given by $eB \sim Z/R^2$, where R is the characteristic length scale proportional to the nuclei radius. For stable nuclei we have $R \sim A^{1/3} \sim Z^{1/3}$ and thus $eB \sim Z^{1/3}$,

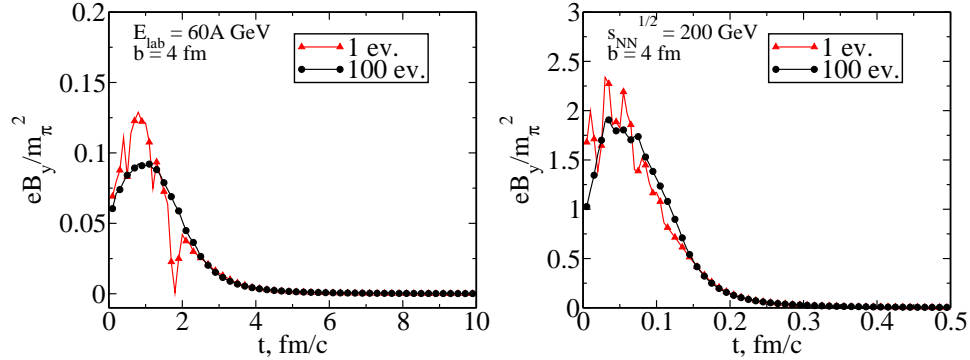


Fig. 2. The time evolution of the magnetic field strength eB_y at the central point O (see Fig.1) in Au–Au collisions with impact parameter $b = 4$ fm in the UrQMD model, in one event (“1 ev.”) and averaged over 100 events (“100 ev.”). The symbols are plotted every $\Delta t = 0.2$ fm/c for $E_{lab} = 60A$ GeV and $\Delta t = 0.01$ fm/c for $\sqrt{s_{NN}} = 200$ GeV.

demonstrating a weak field dependence on the nuclei charge (see similar estimate in Ref. 17).

In Figs. 2 and 3, the time evolution of the magnetic field strength for SPS and RHIC energies is shown. The magnetic field is created in the noncentral Au–Au collision with the impact parameter $b = 4$ fm. The resulting field strength is averaged over 100 events to reduce statistical fluctuations. It is clear, however, that the magnetic field in one individual event can be significant for an observable effect. The nonzero components of the magnetic field strength eB_y in a single event are plotted on the same figures to demonstrate its deviations from the average value, see Fig. 2. In Fig. 3, the magnetic field strength eB_y was estimated also assuming a collision of two uniformly charged Lorenz contracted noninteracting spheres with the radius $R = 7$ fm. The spheres move with the velocity defined by the collision energy. The results obtained in this semianalytical model and the UrQMD one agree to each other. The magnitude of the magnetic field estimated in Ref. 5 for an earlier stage of Au–Au collision at the RHIC energy $\sqrt{s_{NN}} = 200$ GeV and the impact parameter $b = 4$ fm is about $eB \approx 1.3 \cdot m_\pi^2$, which is close to our calculations^b. Note that this magnetic field strength is higher by about 4 orders of magnitude than that in the surface of magnetar²⁴. It is impossible to make steady fields stronger than $4.5 \cdot 10^5$ Gauss in the lab because the magnetic stresses of such fields exceed the tensile strength of terrestrial materials.

In Fig. 4 we show the dependence of the magnetic field strength on the coordinate y for a fixed time corresponding to its maximal value at $y = 0$. As it is seen, the field stays approximately constant up to $y \sim 5$ fm, demonstrating the high degree of homogeneity in the central region.

^bWe measure the magnetic field strength in the units of the pion mass squared, using for definiteness $m_\pi = 140$ MeV. However, the magnetic field strength can be translated into the CGS system

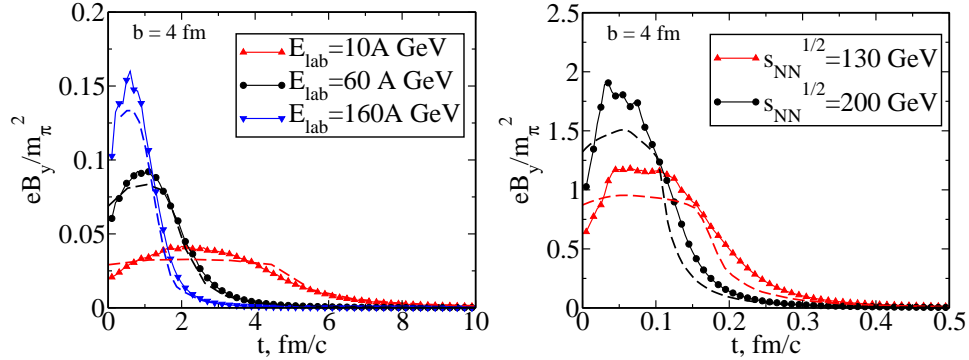


Fig. 3. The time evolution of the magnetic field strength eB_y at the central point O (see Fig.1) in Au–Au collisions with impact parameter, $b = 4$ fm, in the UrQMD model, for different bombarding energies. The symbols are plotted every $\Delta t = 0.2$ fm/c for $E_{lab} = 60A$ GeV and $\Delta t = 0.01$ fm/c for $\sqrt{s_{NN}} = 200$ GeV. The magnetic field obtained by modelling the gold ions as two Lorentz contracted non-interacting uniformly charged spheres with radius $R = 7$ fm are shown by dashed lines.

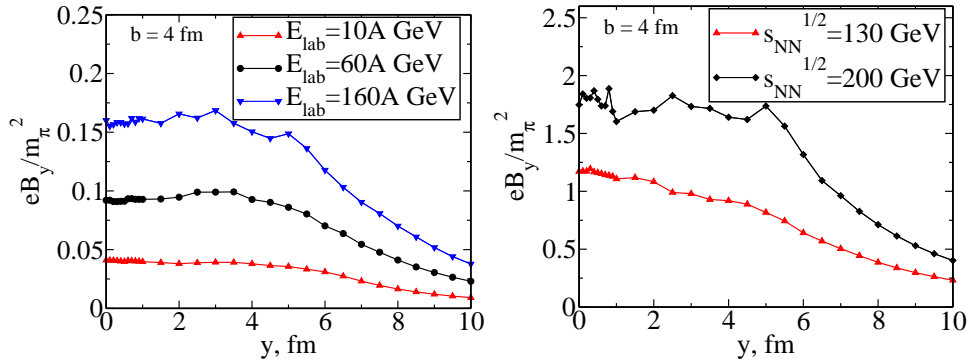


Fig. 4. The dependence of the magnetic field on the coordinate y . The calculation was carried out for Au–Au collisions with impact parameter $b = 4$ fm in the UrQMD model. The magnetic field is taken at fixed time corresponding to its maximum value at $y = 0$.

The large value of the magnetic field strength itself does not guarantee possible observable effects, but additional requirements are needed. For the chiral magnetic effect the system should be in the deconfinement and the chiral restored phase. To demonstrate that matter in the central region is presumably in the QGP phase, we calculate the energy density. We define the center region of the created fireball as a Lorentz contracted box with the transverse and longitudinal size $l_x = l_y = 4$ fm, $l_z = (4/\gamma_{cm})$ fm, where γ_{cm} is a Lorentz factor calculated in the center of mass frame. The energy density is defined as $\varepsilon = E/V_{box}$, where $V_{box} = 64/\gamma_{cm}$ fm³ and

by the following identity $m_\pi^2 = 140^2 \times 0.512 \cdot 10^{14}$ Gauss $\approx 10^{18}$ Gauss.

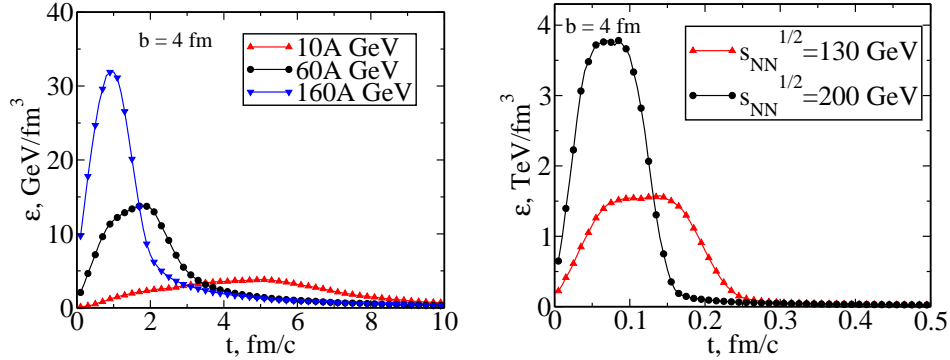


Fig. 5. The time evolution of the energy density in the central region (see text for details) for SPS and RHIC energies.

E is the energy of particles in the box

$$E = \sum_{(x,y,z) \in \text{box}} \sqrt{p_i^2 + m_i^2}. \quad (3)$$

The calculated time evolution of the energy density in the central region is shown in Fig. 5. Even for the bombarding energy $E_{lab} = 10A$ GeV and the impact parameter $b = 4$ fm, the energy density in the central region is sufficient to reach the QGP phase. However, the question whether the system is in local equilibrium and can be described by the temperature and chemical potential(s) is still open. In the framework of the UrQMD model for central collisions the equilibration was considered in Refs. 25,26.

The magnetic field and energy density dependence on the impact parameter are depicted in Fig. 6 for Au–Au collisions at bombarding energies $E_{lab} = 60A$ GeV and $\sqrt{s_{NN}} = 200$ GeV. It is shown that the smaller the impact parameter b the larger the energy density ε and the smaller the magnetic field eB_y is, as it could be expected from simple symmetry considerations.

3. Conclusions

The magnitudes of the magnetic field strength play an important role in estimations of possible observable effects of the deconfinement and chiral phase transitions in heavy-ion collisions. The magnetic field strength in heavy-ion collisions at RHIC energies was estimated by D. Kharzeev, L. McLerran and H. Warringa following simple considerations, see ⁵ for details. For energy $\sqrt{s_{NN}} = 200$ GeV, the authors obtained the magnetic field $eB_y \approx 3 \cdot m_\pi^2$ which is strong enough to provide necessary conditions for the effect to be measured ²⁷. In this paper we employed the UrQMD model for calculation of the magnetic field strength at various bombarding energies $E_{lab} = 10, 60, 160A$ GeV and $\sqrt{s_{NN}} = 130, 200$ GeV. We showed the time evolution of the magnetic field, its dependence on the transverse coordinate y and the impact parameter b . The obtained results demonstrate that the fields emerging

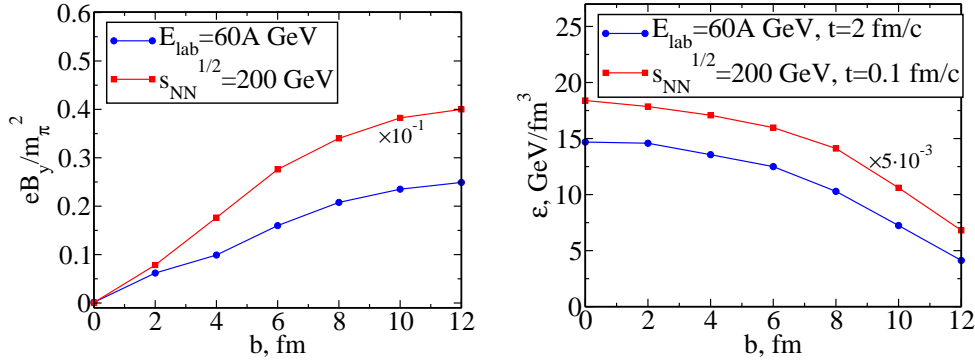


Fig. 6. The magnetic field (left panel) and the energy density (right panel) dependence on the impact parameter b for $E_{\text{lab}} = 60A \text{ GeV}$ and $\sqrt{s_{\text{NN}}} = 200 \text{ GeV}$.

in heavy-ion collision has a high degree of homogeneity in the central region. The analysis of the energy density in the central region allows us to draw the conclusion that the considered system may reach the deconfinement and chiral restored phase. To all appearance, the requirements to observe the chiral magnetic effect are fully satisfied. We compared the UrQMD calculations with a simple semianalytical model considering heavy ions as two Lorenz-contracted uniformly-charged noninteracting spheres. The semianalytical results are in a satisfactory agreement with the dynamical ones. The former underestimate the UrQMD calculations by only few percent. Using this model we can estimate the lowest bound of the maximal magnetic field strength at the LHC energy $\sqrt{s_{\text{NN}}} = 4.5 \text{ TeV}$ to be about $15 \cdot m_\pi^2$ in collisions of Pb–Pb ions with the impact parameter $b = 4 \text{ fm}$, which is twice higher than that estimated in Ref. ¹⁰.

4. Acknowledgements

We are grateful to K.K. Gudima, E.E. Kolomeitsev and D.N. Voskresensky for criticism and valuable discussions. We are thankful to D.E. Kharzeev and O.V. Teryaev for reading the manuscript. V.S. and V.T. were partially supported by the Bundesministerium für Bildung und Forschung (BMBF project RUS 08/038). V.S. acknowledges the support of the RFBR grant No. 08-02-01003-a and V.T. acknowledges the Heisenberg-Landau grant support.

References

1. L. McLerran and R. D. Pisarski, Nucl. Phys. A **796**, 83 (2007) [arXiv:0706.2191].
2. Y. Hidaka, L. D. McLerran and R. D. Pisarski, Nucl. Phys. A **808**, 117 (2008) [arXiv:0803.0279].
3. A. Bazavov *et al.*, arXiv:0903.4379.
4. Y. Aoki, S. Borsanyi, S. Durr, Z. Fodor, S. D. Katz, S. Krieg and K. K. Szabo, arXiv:0903.4155.

5. D. E. Kharzeev, L. D. McLerran and H. J. Warringa, Nucl. Phys. A **803**, 227 (2008) [arXiv:0711.0950].
6. K. Fukushima, D. E. Kharzeev and H. J. Warringa, Phys. Rev. D **78**, 074033 (2008) [arXiv:0808.3382].
7. V. P. Gusynin, V. A. Miransky and I. A. Shovkovy, Phys. Rev. D **52**, 4747 (1995) [arXiv:hep-ph/9501304].
8. T. D. Cohen, D. A. McGady and E. S. Werbos, Phys. Rev. C **76**, 055201 (2007) [arXiv:0706.3208].
9. P. V. Buividovich, M. N. Chernodub, E. V. Luschevskaya and M. I. Polikarpov, arXiv:0812.1740.
10. E. S. Fraga and A. J. Mizher, Phys. Rev. D **78**, 025016 (2008) [arXiv:0804.1452].
11. A. J. Mizher and E. S. Fraga, Nucl. Phys. A **820**, 247 (2009) [arXiv:0810.4115].
12. N. O. Agasian and S. M. Fedorov, Phys. Lett. B **663**, 445 (2008) [arXiv:0803.3156].
13. A. Ayala, A. Bashir, A. Raya and A. Sanchez, arXiv:0904.4533.
14. M. G. Alford, J. Berges and K. Rajagopal, Nucl. Phys. B **571**, 269 (2000) [arXiv:hep-ph/9910254].
15. K. Fukushima and H. J. Warringa, Phys. Rev. Lett. **100**, 032007 (2008) [arXiv:0707.3785].
16. J. L. Noronha and I. A. Shovkovy, Phys. Rev. D **76**, 105030 (2007) [arXiv:0708.0307].
17. D. N. Voskresensky and N. Y. Anisimov, Sov. Phys. JETP **51**, 13 (1980) [Zh. Eksp. Teor. Fiz. **78**, 28 (1980)].
18. D. T. Son and A. R. Zhitnitsky, Phys. Rev. D **70**, 074018 (2004) [arXiv:hep-ph/0405216].
19. M. A. Metlitski and A. R. Zhitnitsky, Phys. Rev. D **72**, 045011 (2005) [arXiv:hep-ph/0505072].
20. D. T. Son and M. A. Stephanov, Phys. Rev. D **77**, 014021 (2008) [arXiv:0710.1084].
21. N. Sadooghi, arXiv:0905.2097.
22. S. A. Bass *et al.*, Prog. Part. Nucl. Phys. **41**, 255 (1998) [arXiv:nucl-th/9803035].
23. M. Bleicher *et al.*, J. Phys. G **25**, 1859 (1999) [arXiv:hep-ph/9909407].
24. <http://solomon.as.utexas.edu/~duncan/magnetar.html> .
25. L. V. Bravina *et al.*, Phys. Rev. C **60**, 024904 (1999) [arXiv:hep-ph/9906548].
26. L. Bravina *et al.*, Int. J. Mod. Phys. E **16** (2007) 777.
27. S.A. Voloshin, Phys. Rev. C **62**, 044901 (2000) [arXiv:nucl-th/0004042].